LLNL-TR-416095

LAWRENCE
LIVERMORE
NATIONAL
LABORATORY

Continuum level formulation and implementation of a multi-scale model for vanadium

R. Becker, A. Arsenlis, J. Marian, M. Rhee, M. Tang and L. Yang

August, 2009

This document was prepared as an account of work sponsored by an agency of the United States government. Neither the United States government nor Lawrence Livermore National Security, LLC, nor any of their employees makes any warranty, expressed or implied, or assumes any legal liability or responsibility for the accuracy, completeness, or usefulness of any information, apparatus, product, or process disclosed, or represents that its use would not infringe privately owned rights. Reference herein to any specific commercial product, process, or service by trade name, trademark, manufacturer, or otherwise does not necessarily constitute or imply its endorsement, recommendation, or favoring by the United States government or Lawrence Livermore National Security, LLC. The views and opinions of authors expressed herein do not necessarily state or reflect those of the United States government or Lawrence Livermore National Security, LLC, and shall not be used for advertising or product endorsement purposes.

This work performed under the auspices of the U.S. Department of Energy by Lawrence Livermore National Laboratory under Contract DE-AC52-07NA27344.

Continuum level formulation and implementation of a multi-scale model for vanadium

R. Becker, A. Arsenlis, J. Marian, M. Rhee, M. Tang and L. Yang

Lawrence Livermore National Laboratory
7000 East Avenue, P.O. Box 808, Livermore, CA 94550

Abstract

A multi-scale approach is used to construct a continuum strength model for vanadium. The model is formulated assuming plastic deformation by dislocation motion and strain hardening due to dislocation interactions. Dislocation density is adopted as the state variable in the model. Information from molecular statics, molecular dynamics and dislocation dynamics simulations is combined to create kinetic relations for dislocation motion, strain hardening relations and evolution equations for the dislocation density. Implicit time integration of the constitutive equations is described in the context of implementation in a finite element code. Results are provided illustrating the strain, strain rate, temperature and pressure dependence of the constitutive model.

Introduction

The Physics and Engineering Materials program at LLNL has been working toward multiscale modeling of material strength for nearly a decade. Much of that time was spent developing and validating simulation capabilities accounting for mechanisms at various length scales. Over the past few years there has been a concerted effort to combine information from the different length scales to produce a multiscale strength model. The first attempt at a bottom to top integration across the length scales was a model for tantalum presented as a FY-2007, L2 PEM Milestone[1]. A year later a second multiscale strength milestone was completed for vanadium[2] . This model improved the linking of scales in several crucial areas. The purpose of this report is to provide a more detailed description of the resulting continuum model for vanadium.

The vanadium multiscale strength model was constructed using an information passing paradigm where simulation results from one size scale were used to define functional forms and parameters that served as the basis for the model at the next larger length scale. The process starts with density functional theory, and includes molecular statics, molecular dynamics, and dislocation dynamics simulations. Model forms and parameters are determined at each level. In this report, only the results from simulations that feed directly into the macroscale continuum model are described. The models generating the results and the simulations at lower length scales are cited and are discussed elsewhere.

Model Construction

The presumed basis for the macroscale model is plastic deformation by thermally activated dislocation motion and strain hardening resulting from elastic interactions among dislocations. The connection between dislocation mechanics and macroscale plasticity variables is through traditional models. Dislocation density is evolved as the state variable that characterizes the flow strength of the material. The primary focus for the current model is the temperature, strain rate and pressure dependence of the plastic flow strength. Microstructure and mechanisms at the grain scale are neglected, and the material is assumed to be isotropic following J2-Flow theory plasticity with an associative flow rule.

Connection to continuum variables

Orowan's equation gives the macroscale plastic strain rate, $\dot{\varepsilon^p}$, in terms of mean dislocation velocities, v, and dislocation densities, ρ.

$$\dot{\varepsilon^p} = \frac{b}{M}(\rho_e v_e + \rho_s v_s) \tag{1}$$

Here, b is the Burgers vector of the bcc vanadium crystal, M is the Taylor factor accounting for the average crystal orientation, and the subscripts e and s denote edge and screw dislocation populations, respectively. While moving dislocations have a wide range of velocities, nominal average values are employed for the current model.

The thermally activated dislocation motion is driven by the net resolved shear stress on a particular slip system. This net shear stress, τ^*, is given in terms of the von Mises effective stress, $\bar{\sigma}$, the Taylor factor and the athermal strength, τ_a:

$$\tau^{*s} = \frac{\bar{\sigma}}{M} - \tau_a^s \tag{2}$$

The athermal strength, defined in Eq. 19 below, is different for the edge and screw dislocations, so the net resolved shear stress can also vary with dislocation character.

Use of these historical linking assumptions bypasses mechanisms on the grain scale and neglects effects of grain boundaries on dislocation propagation and strength. It is recognized that the Hall-Petch effect and other mechanisms at the grain scale can have a significant impact on measured strength, but the compressed time scale for model development necessitated omission of simulations on certain length scales.

Kinetic model driving force from molecular statics calculations

The energy barrier for dislocation motion can be overcome by a combination of shear stress and thermal activation. The thermally activated dislocation velocity is assumed to follow an Arrhenius relation,

$$v = v_0 \exp\left(\frac{-H}{kT}\right) \tag{3}$$

where H is an activation energy barrier, v_0 a reference velocity, T the absolute temperature and k Boltzmann's constant. The activation energy in Eq. 3 is assumed to be a function of resolved shear stress and pressure, and these dependencies are determined by molecular statics calculations at 0K [3,4]. Figure 1 shows results from the molecular statics simulations for both screw and edge dislocations at three pressures. The lines represent the height of the energy barrier after application of shear stress. This is the barrier that must be overcome by thermal mechanisms. Also shown are fits to the numerical data. The fitting process is described below.

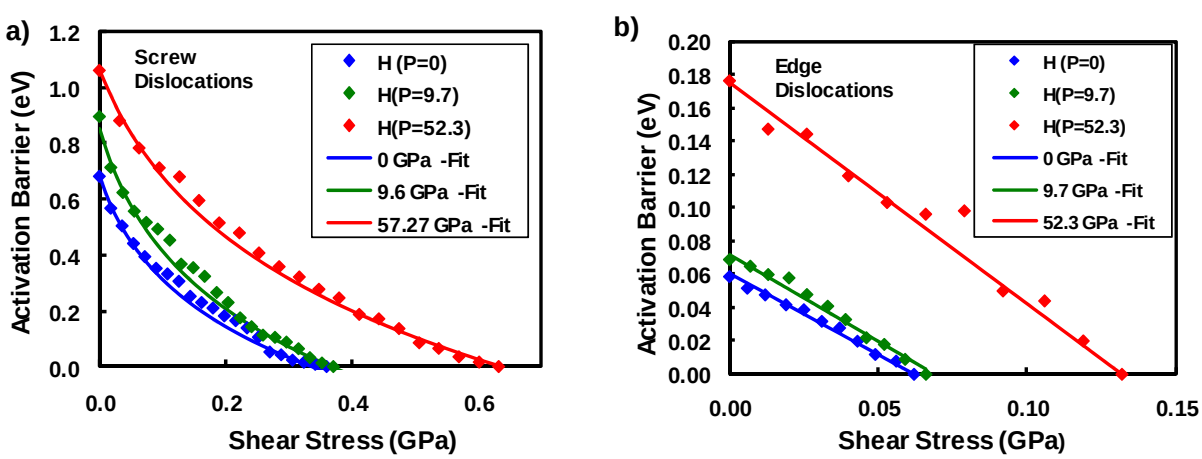

Figure 1. Activation energy for a) screw and b) edge dislocations predicted from molecular statics calculations (symbols) and the corresponding model fits (lines) at 3 pressures.

Assuming that the activation energy is a multiplicative function of shear stress and pressure, the pressure dependence of the activation energy is determined by fitting a quadratic function to the numerical data at zero shear stress for both the screw and edge dislocations. The pressure, p, is normalized by the reference shear modulus, G_0.

$$\frac{H_0^s}{k}(°K) = 7891 + 11292\left(\frac{p}{G_0}\right) - 6700\left(\frac{p}{G_0}\right)^2 \tag{4a}$$

$$\frac{H_0^e}{k}(°K) = 696 + 579\left(\frac{p}{G_0}\right) - 630\left(\frac{p}{G_0}\right)^2 \tag{4b}$$

Similarly, fitting the numerical data from Figure 1 at zero on the vertical axis gives the pressure dependence of the shear stress required to move dislocations in the absence of thermal activation. This is the Peierls stress, τ_p, and it is fit by

$$\tau_p^s = G_0\left[0.006939 + 0.0018786\left(\frac{p}{G_0}\right) + 0.003530\left(\frac{p}{G_0}\right)^2\right] \tag{5a}$$

$$\tau_p^e = G_0\left[0.001265 + 0.000518\left(\frac{p}{G_0}\right) + 0.000711\left(\frac{p}{G_0}\right)^2\right] \tag{5b}$$

With the end points of the curves in Figure 1 specified by Eqs 4 and 5, functions are constructed fitting the data in between. These are, for screw and edge dislocations, respectively:

$$H^s = H_0^s \ \ln\left(\frac{1+\alpha}{\tau^{*s}/\tau_p^s + \alpha}\right)\Big/\ln\left(\frac{1+\alpha}{\alpha}\right) \ \ ; \ \ \alpha = 0.14 \tag{6a}$$

$$H^e = H_0^e \ \left(1 - \frac{\tau^{*e}}{\tau_p^e}\right) \tag{6b}$$

It is significant that the reference activation energies and the Peierls stresses in Eqs 4 and 5 are fit using only the reference shear modulus ($G_0 = 49000$ MPa) rather than the pressure and temperature dependent shear modulus. Figure 2 shows the calculated reference activation energy and Peierls stress normalized by the pressure-dependent shear modulus plotted as a function of pressure. While the normalization by the pressure dependent modulus appears to capture the pressure dependence of the screw dislocations, the pressure dependence of the edge dislocations is not well represented. This is likely because an edge dislocation is dilational, and creation of an

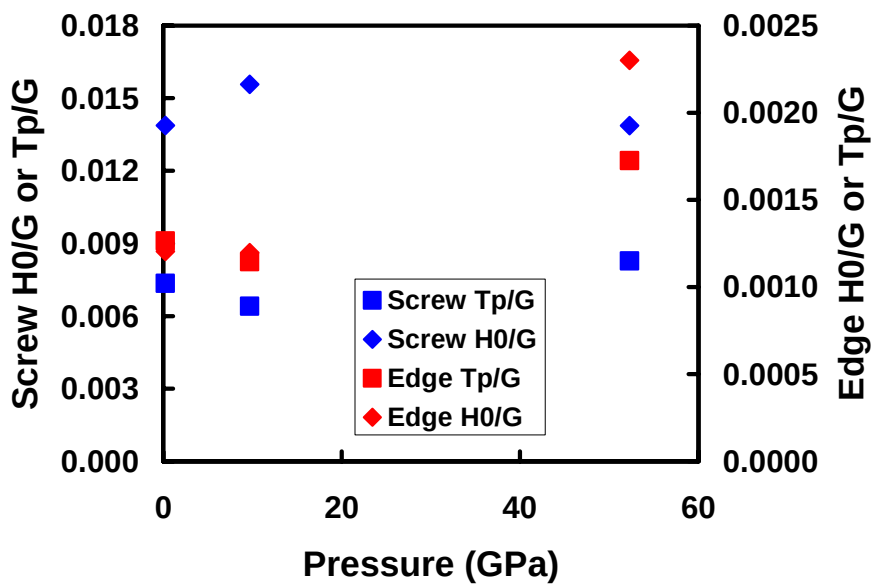

Figure 2. Reference activation energy and Peierls stress for edge and screw dislocations as a function of pressure.

edge dislocation does work against the applied pressure. This additional work is not captured by shear modulus scaling, but the effect is captured through Eqs 4 and 5.

While the pressure dependent shear modulus could have been used in Eqs 4 and 5, an additional pressure correction would be needed. That would increase the complexity of the model unnecessarily, add parameters, and tie the parameterization of the strength model to the particular shear modulus model used when fitting the data. Changes to the shear modulus model would then require reparameterization of the strength model. This is not a desirable model construct.

Kinetic parameters from molecular dynamics calculations

Molecular dynamics simulations, similar to those in [5,6], were used to determine kinetic relations for edge and screw dislocation in vanadium at a range of temperatures from 200K-1000K. Guided by the common assumption that dislocation motion is affected by thermal activation at low stress and by phonon drag at high stress, functional forms were fit in the two regimes and a smooth transition function was applied. At lower stress, Arrhenius equations were applied in both forward and backward directions so the dislocation velocity is zero at zero stress. The dislocation velocities are fit well by linear stress dependence in the phonon drag regime, and the functional form for the transition region is simply a curve fit. Figure 3 shows the molecular dynamics results and the parameterized fits.

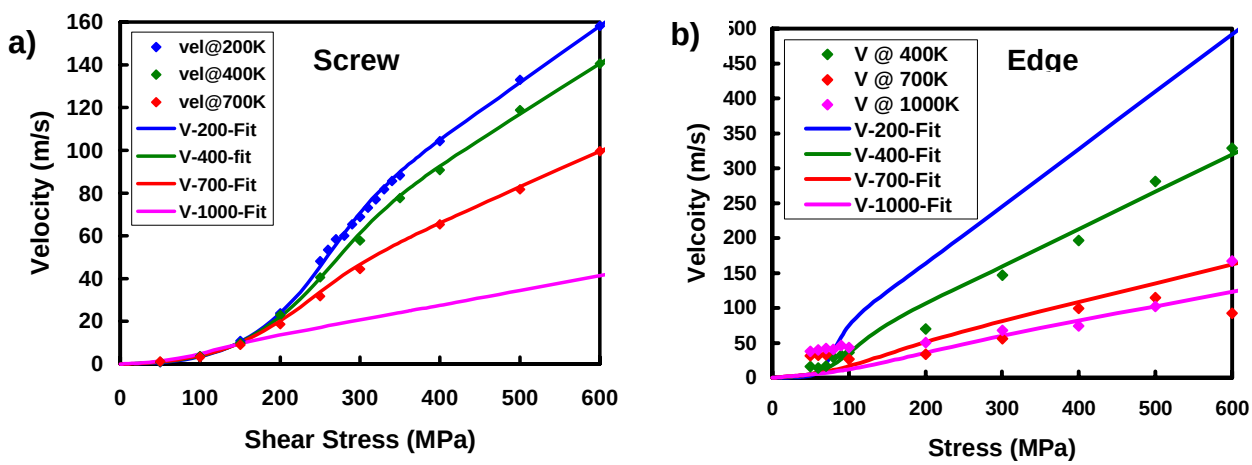

Figure 3. a) screw and b) edge dislocation velocities predicted by molecular dynamics simulations and the accompanying curve fits.

The fit for the screw dislocation velocities is given by expressions for the thermally activated and drag regimes and the transition function.

$$v^s = \frac{v^s_{Therm}\, v^s_{Drag}}{\sqrt[1/5]{(v^s_{Therm})^5 + \left(v^s_{Drag}\right)^5}} \tag{7}$$

$$v^s_{Drag} = \xi^s_D C_0 \frac{\tau^{*s}}{\tau^s_p} \tag{8}$$

$$v^s_{Therm} = \xi^s_T\, C_0 \left[\exp\left(-\beta^s \frac{H^s}{kT}\right) - \exp\left(-\beta^s \frac{H^{*s}}{kT}\right)\right] \tag{9}$$

The activation energy in the reverse direction, H^{*s}, is limited to prevent numerical underflow as the backward velocity contribution goes to zero.

$$H^{*s} = \begin{cases} H(-\tau) & \tau \leq 0.95\,\alpha\,\tau_p^s \\ H\left(0.95\,\alpha\,\tau_p^s\right) & \tau > 0.95\,\alpha\,\tau_p^s \end{cases} \tag{10}$$

In the screw dislocation kinetic relations, $C_0 = 5077\ m/s$ is a reference sound speed and the remaining parameters are functions of temperature

$$\begin{aligned} \beta^s &= 0.019426 + 9.115 \times 10^{-4} T - 1.3776 \times 10^{-7} T^2 \\ \xi_T^s &= 0.03100 - 3.650 \times 10^{-5} T + 2.3030 \times 10^{-8} T^2 \\ \xi_D^s &= 0.018788 - 3.484 \times 10^{-6} T - 1.0695 \times 10^{-8} T^2 \end{aligned} \tag{11}$$

It is important to note that the $\beta^s$and ξ_T^s parameters differ significantly from unity and have a significant temperature dependence. Good fits could not be constructed with constant values. This implies that the thermally activated screw dislocation velocities are not well represented by the assumptions underlying the Arrhenius relation. It is likely because energy barrier heights are temperature dependent.

Expressions for the edge dislocation velocities are similar, but the fit in the thermally activated regime is contrived. The molecular dynamics simulations were extremely noisy at low stress and the numerical data are not meaningful. The numerical data in the phonon drag range are well behaved.

$$v^e = \frac{v_{therm}^e\, v_{Drag}^e}{\sqrt[1/3]{\left(v_{Therm}^e\right)^3 + \left(v_{Drag}^e\right)^3}} \tag{12}$$

$$v_{Therm}^e = \xi_T^e\, C_0 \exp\left(-\beta^e \frac{H^e}{kT}\right) \sinh\left(\beta^e \frac{H^e}{kT} \frac{\tau^{*e}}{\tau_p^e}\right) \tag{13}$$

$$v_{Drag}^e = \xi_D^e C_0 \frac{\tau^{*e}}{\tau_p^e} \tag{14}$$

Since the stress dependence in the Arrhenius equation is linear for the edge dislocation, the forward and backward dislocation velocities combine to give the hyperbolic sine dependence. The parameterization of the remaining constants is simpler for the edge dislocations in the thermal regime since they are simply postulated rather than fit to molecular dynamics data.

$$\begin{aligned} \beta^e &= 2 \\ \xi_T^e &= 0.05 \\ \xi_D^e &= 0.0145 - 2.53 \times 10^{-5} T - 1.33 \times 10^{-8} T^2 \end{aligned} \tag{15}$$

Density evolution from dislocation dynamics simulations

The kinetic relations described above were implemented in the ParaDiS [7,8] dislocation dynamics code to simulate the evolution of dislocation density and strain hardening. The predicted dislocation density evolution was then used to parameterize evolution equations for the continuum hardening model.

The continuum dislocation density evolution model is based on existing dislocation growth and capture radii relations, and a dislocation multiplication term is tacked on to force

homogeneous dislocation nucleation at high stresses. The physical motivation for the growth relations is based on a simple dislocation loop growth model. The increase in screw dislocation length depends on the velocity of the edge dislocation segments; and, likewise, increases in edge dislocation density depend on screw dislocation velocity. Dislocation density decreases are presumed to result from capture of oppositely signed dislocations within a capture radius, R_c. The capture radius depends on the velocity of the passing dislocations, but it is parameterized in terms of stress in Eqs 17 for convenience. Finally, the homogeneous nucleation term at the end is simply a construction that has negligible contribution at low stress and generates appreciable dislocation density as the stress approaches the ideal strength of the crystal. Here it is assumed that $\mathrm{T}_{ideal} = 0.1\, G_0$.

$$\dot{\rho_s} = \frac{2\rho_e\, v^e}{l_e} - \rho_s^2 R_{cs} v^s + \frac{0.01 v^s}{b^3} \exp\left[-15\left(1 - \frac{\tau}{\tau_{Ideal}}\right)\right] \tag{16a}$$

$$\dot{\rho_e} = \frac{2\rho_s\, v^s}{l_s} - \rho_e^2 R_{ce} v^e + \frac{0.01 v^e}{b^3} \exp\left[-15\left(1 - \frac{\tau}{\tau_{Ideal}}\right)\right] \tag{16b}$$

The capture radius was adjusted until the dislocation density evolution predicted by Eq. 16 matched that given by ParaDiS. The capture radii from 13 simulations at different strain rates, temperatures and pressures were plotted as a function of stress and used to fit the expressions.

$$R_{cs} = 461.39 \exp\left(-1.2138 \frac{\tau}{\tau_p}\right) + 1 \tag{17a}$$

$$R_{ce} = 113.84 \exp\left(-213.98 \frac{\tau}{G_0}\right) + 1 \tag{17b}$$

The simulation data and the model fits are shown in Figure 4. As the stress and dislocation velocity increase, the dislocations spend less time in locations where they can be captured and the capture radius decreases. It can be noted that the stress normalization is done differently for the screw and edge relations. The screw relation scales with the Peierls stress which scales with shear modulus for the screw dislocations. The edge expression, on the other hand, did not scale as well with the associated Peierls stress, so it was simply a normalized by the reference shear modulus.

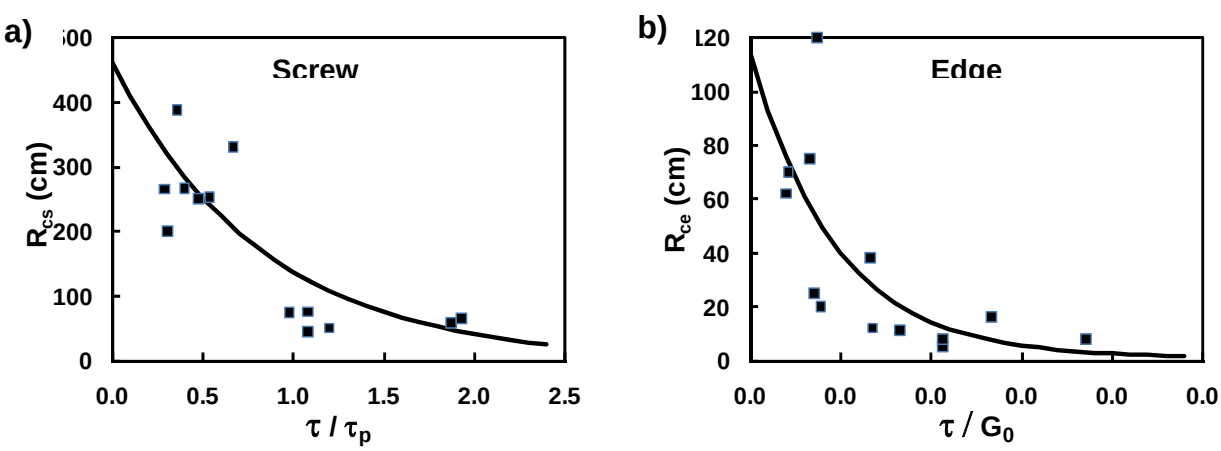

Figure 4. Fits to calculated capture radius data for a) screw and b) edge dislocations.

The other material state variable in these evolution relations is the dislocation link length, l. It increases as the dislocation loops expand and decreases as dislocations from other systems intersect and produce shorter segments. As with the dislocation evolution equations, the link length evolution expressions are motivated by single loop concepts.

$$\dot{l_s} = \frac{l_s}{\rho_s}\,\dot{\rho_s} - 0.002 l_s^3\,\dot{\rho_e} \tag{18a}$$

$$\dot{l_e} = \frac{l_e}{\rho_e}\,\dot{\rho_e} - 0.002 l_e^3\,\dot{\rho_s} \tag{18b}$$

The combined set of dislocation evolution equations has few tunable parameters. A typical fit for dislocation density is shown in Figure 5.

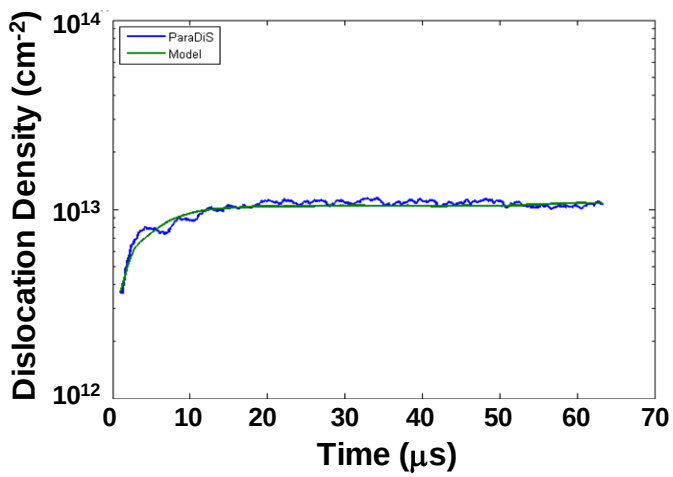

Figure 5. Predicted screw dislocation density evolution and the model fit.

Additional information extracted from the dislocation dynamics simulations is the effect of dislocation density on strength. Assuming the traditional square root dependence of strength on dislocation density, interaction coefficients are determined by fitting the simulated strength data.

$$\tau_a^s = 0.321\, Gb\sqrt{\rho_s + \rho_e} + \tau_{a0}^s \tag{19a}$$

$$\tau_a^e = 0.415\, Gb\sqrt{\rho_s + \rho_e} + \tau_{a0}^e \tag{19b}$$

The coefficients are on the order of experimentally determined values cited in the literature. An offset value, τ_{a0}, of 10 MPa was added to the athermal stress for both screw and edge to ensure a finite lower limit even if initial dislocation densities were set very low.

Using a traditional equation tying dislocation density to strength carries an additional assumption which needs to be investigated through further simulations—namely, the strength dependence on shear modulus. Choosing the model form of Eq. 19 implies that, for a given microstructure state, the temperature and pressure dependence of the strength scales with the shear modulus. This is one of the very assumptions that the multiscale strength simulations should be investigating, so it should not be assumed in the model form. Future model

development efforts must examine the relationship between dislocation density and strength more thoroughly.

Model simplifications for numerical stability and additional data constraints

The relations outlined above were implemented and several issues were uncovered. The coupling between the edge and screw dislocation density evolution rates is very strong and highly nonlinear. Extremely small time steps are required for stability and to capture the path dependence. Several semi-implicit and subcycling algorithms were tried, but none gave stability and accuracy at a time step tractable in an explicit finite element code. In addition, certain sets of initial conditions or load paths resulted in unphysical behavior such as plastic deformation occurring entirely by motion of screw dislocations with no edge dislocation velocity. These responses are believed to have resulted from insufficient direct coupling between the evolution of screw and edge dislocation densities. Equations 16 specify screw and edge dislocation density evolution, but there is nothing in the formulation to enforce a coordinated evolution of the two populations.

The machinery of the dislocation dynamics model provides coordinated dislocation density evolution, so a path forward was suggested by further examination of the ParaDiS results. The fraction of screw dislocations is about 0.6 over a wide range of loading conditions and dislocation densities, Figure 6. Therefore, a modification to the continuum model ties the edge dislocation evolution to the screw component so that $\rho_e = 2\rho_s/3$. As a consequence, the modified model is ultimately formulated entirely in terms of the screw dislocation density and velocity. When needed, the edge density is simply calculated and inserted. The edge dislocation link length in Eq. 16a is determined by integrating Eq. 18b using the 2/3 restriction on the edge density and rate.

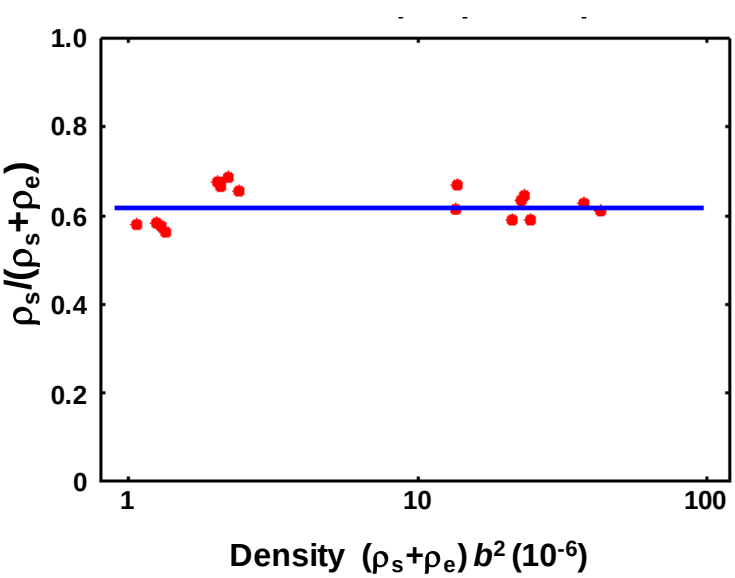

Figure 6. Fraction of screw dislocations for a range of strains and deformation conditions.

A further assumption is needed to determine an edge dislocation velocity consistent with the screw velocity. There are several approaches to calculating a consistent edge velocity; the path chosen presents little opportunity for instabilities or other issues. Say there is finite, steady slip along any given slip system at a macroscopic level. This is a simple, rigid translation of the

crystal above the slip plane with respect the crystal below the slip plane. If all dislocations initiate as loops at the center of the slip plane, the fluxes of edge and screw dislocations must be equal for steady state crystal slip. This equal flux assumption, $\rho_e v^e = \rho_s v^s$, is used in calculating the evolution rate for screw dislocations using Eq. 16a and the strain rate in Eq. 1. The edge kinetic relations and the evolution equations for edge dislocations are not used.

Model implementation

The model was implemented in the Arbitrary Lagrange Eulerian code ALE3D. At the highest level of the material model integration scheme, iterations are performed to determine the stress commensurate with the applied deformation and the elasticity. Integration of the dislocation density, Eq. 16a, is through a combination of backward implicit iteration and closed form integration assuming a constant link length, l_e, over a time step. Finally, the dislocation link length is integrated in closed form given the density evolution rate. The link length evolves slowly compared to the dislocation density, so using the value from the beginning of the time step in the density evolution equation is a reasonable approximation

Coupling to the elasticity relations

For J2-Flow theory with an associative flow rule, the scalar relation coupling the elastic and plastic deformation is

$$\bar{\sigma} + 3G\Delta t\dot{\varepsilon}^p(\bar{\sigma}, T, p, \rho_s, \rho_e) = \sigma_e^{Tr} \tag{20}$$

where $\bar{\sigma}$ is the von Mises or equivalent stress

$$\bar{\sigma} = \sqrt[2]{\frac{2}{3}\left(\sigma_{ij}\,\sigma_{ij}\right)} \tag{21}$$

and the effective trial stress, σ_e^{Tr}, is given in terms of the deviatoric stress at the beginning of the time step and the total deviatoric strain increment, $\Delta\varepsilon'_{ij}$, by

$$\sigma_e^{Tr} = \sqrt[2]{\frac{2}{3}\left(\sigma_{ij}^{Tr}\,\sigma_{ij}^{Tr}\right)} \tag{22}$$

$$\sigma_{ij}^{Tr} = \sigma'_{ij_t} + 2G\Delta\varepsilon'_{ij} \tag{23}$$

The prime in Eq. 23 denotes the deviatoric part of the tensor. The plastic strain rate in Eq. 20 depends on the equivalent stress, temperature and history variables through the relations presented above.

Equation 20 is solved iteratively for the equivalent stress using a combined Newton-Raphson iteration and bisection method. The lower bound on the stress is taken as the yield value and the upper bound is the effective trial stress. There are potentially issues with the lower limit if softening due to dislocation annihilation exceeds the increased strength due to rate dependence, but this has not been encountered so far. A more robust solution would have the stress represented in terms of the strain rate, but that is not feasible with the current model structure.

Dislocation density calculation

The multiscale constitutive routine calculates the plastic strain rate given the estimate of the equivalent stress. The thermally activated shear stress is determined by Eq. 2 where the athermal stress is given by Eq. 19a. The ratio of the shear stress to the Peierls stress is used to determine

the activation energy in Eq. 6 and the screw dislocation velocity is calculated using Eqs 7-11. Using the assumption $\rho_e v^e = \rho_s v^s$ described above, the screw evolution expression, Eq. 16a, is rewritten

$$\frac{d\rho_s}{N + M\rho_s - A\rho_s^2} = dt \tag{24}$$

where

$$A = -R_{cs} v^s \; ; \quad M = \frac{2v^s}{l_e} \; ; \quad N = \frac{0.01 v^s}{b^3} \exp\left[-15\left(1 - \frac{\tau}{\tau_{Ideal}}\right)\right] \tag{25}$$

Equation 24 can be solved in closed form over the time increment as

$$\rho_s = \frac{M[(M - 2A\rho_{st})(1 - E) - q(1 + E)] + q[(M - 2A\rho_{st})(1 + E) - q(1 - E)]}{2A[(M - 2A\rho_{st})(1 - E) - q(1 + E)]} \tag{26}$$

with

$$q = \sqrt[2]{M^2 + 4AN} \qquad \text{and} \qquad E = \exp(-q\Delta t) \tag{27}$$

This closed form integration is unconditionally stable and valid for any size time step. It returns the dislocation density at the beginning for the time step, ρ_{st}, for a zero time step and approaches the saturation density at as the time step approaches infinity.

There is a complication because Eq. 26 is used in a full backward integration scheme for the plastic strain rate; the dislocation velocity appearing in the coefficients of Eq. 26 depends on the dislocation density. This creates an implicit dependence on ρ_s that is resolved through iteration. Writing the error in the dislocation density as the assumed value used to calculate coefficients in Eq. 26 minus the value computed by Eq. 26 gives an error that can be driven to zero with the Newton iteration method.

$$\rho_{err} = \rho_s - \hat{\rho}\left(\tau, v^s\left(\tau^{*s}(\rho_s, \tau)\right)\right) \tag{28}$$

A linearization of Eq. 28 provides an equation to solve for a correction to dislocation density.

$$0 = \rho_s - \hat{\rho}\left(\tau, v^s(\tau^{*s}(\rho_s, \tau)\,)\right) + \left[1 - \frac{\partial\hat{\rho}}{\partial v^s}\frac{dv^s}{d\tau^{*s}}\frac{\partial\tau^{*s}}{\partial\rho_s}\right]\delta\rho_s - \left[\frac{\partial\hat{\rho}}{\partial\tau} + \frac{\partial\hat{\rho}}{\partial v^s}\frac{dv^s}{d\tau^{*s}}\frac{\partial\tau^{*s}}{\partial\tau}\right]\delta\tau \tag{29}$$

The applied stress, τ, is fixed by the iterations over Eq. 20. Therefore, the variation in applied stress, $\delta\tau$, is zero when calculating the plastic strain rate in the multiscale constitutive routine. With $\delta\tau = 0$, Eq. 29 provides the expression for the correction to dislocation density used in the Newton-Raphson iteration.

$$\delta\rho_s = \frac{-\rho_{err}}{1 - \frac{\partial\hat{\rho}}{\partial v^s}\frac{dv^s}{d\tau^{*s}}\frac{\partial\tau^{*s}}{\partial\rho_s}} \tag{30}$$

For a given value of τ, Eq. 30 is evaluated and the dislocation density updated until the error reaches an acceptable tolerance. Limits are placed on the dislocation density correction so that it never exceeds 25% of the current dislocation value. Also, the resulting density can't be so high as to set the driving force, τ^{*s}, to zero. A maximum permitted dislocation density is calculated from τ for this purpose. This limit is approached gradually to prevent oscillations in the solution. With ρ_s determined, the dislocation velocities and edge dislocation density are easily computed.

The edge dislocation link length can likewise be integrated in closed form once the change in dislocation density is known. Here the increment in edge dislocation density is assumed to be 2/3 that of the screw increment. The screw segment length is not needed and not computed.

$$l_e = \sqrt{\frac{l_{s0}^2 \ \exp(2\Delta\rho_s/\rho_s)}{1 + 0.002\rho_s l_{s0}^2 \exp(2\Delta\rho_s/\rho_s)}} \tag{31}$$

Plastic strain rate and derivatives

With the dislocation density and velocity determined as outlined above, the plastic strain rate is computed from Eq. 1, again assuming that the edge and screw dislocation fluxes are equal, $\rho_e v_e = \rho_s v_s$. Remaining is to compute the derivative of the plastic strain rate with respect to stress needed for the Newton-Raphson iteration on Eq. 20. This is given by

$$\frac{d\dot{\varepsilon}^p}{d\bar{\sigma}} = \left[\frac{\partial\dot{\varepsilon}^p}{\partial\rho_s}\frac{d\rho_s}{d\tau} + \frac{\partial\dot{\varepsilon}^p}{\partial v^s}\frac{dv^s}{d\tau^{*s}}\left(\frac{\partial\tau^{*s}}{\partial\tau} + \frac{\partial\tau^{*s}}{\partial\rho_s}\frac{d\rho_s}{d\tau}\right)\right]\frac{d\tau}{d\bar{\sigma}} \tag{32}$$

Since the error indicated by Eq. 28 has been driven toward zero and should remain zero, the rate of change of dislocation density with stress can be determined from Eq. 29 as:

$$\frac{d\rho_s}{d\tau} = \left[\frac{\partial\hat{\rho}}{\partial\tau} + \frac{\partial\hat{\rho}}{\partial v^s}\frac{dv^s}{d\tau^{*s}}\frac{\partial\tau^{*s}}{\partial\tau}\right] \Big/ \left[1 - \frac{\partial\hat{\rho}}{\partial v^s}\frac{dv^s}{d\tau^{*s}}\frac{\partial\tau^{*s}}{\partial\rho_s}\right] \tag{33}$$

The remaining derivatives used in Eq. 32 are straight forward to calculate.

Model Behavior

Single element, adiabatic, uniaxial stress simulations were run over a wide range of strain rates, temperatures and pressures to ensure that the model gives physically plausible results and is numerically robust. Selected results are provided below to illustrate the model behavior.

The strength depends on both the dislocation density and the dislocation velocity through the kinetic relations, and the two effects are intricately coupled. Increased strength with increasing strain rate from the kinetic relation reduces the dislocation capture radius leading to a higher dislocation density and still higher strength. Figure 7a shows dislocation density evolution for strain rates from 10^{-6} sec^{-1} to 10^{8} sec^{-1}. There is little effect of strain rate at lower strain rates, but

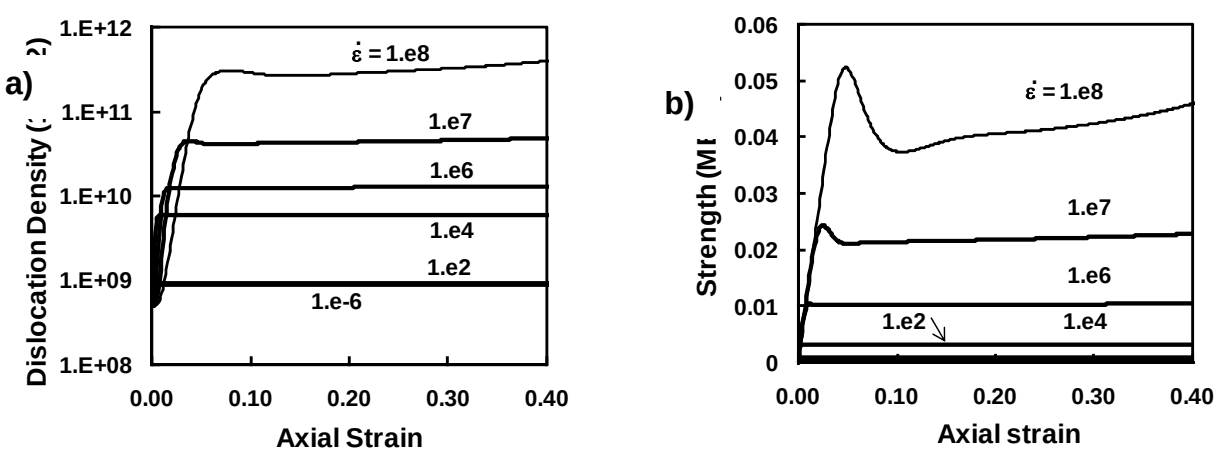

Figure 7. Evolution of a) dislocation density and b) strength at a variety of strain rates for ambient pressure and initial temperature of 300K.

increases of dislocation density with strain rate are substantial at higher rates. This is reflected in the strength evolution, Figure 7b, where the strength also increases substantially at higher rates.

The dislocation density evolves rapidly and saturates at low to moderate strains resulting in little strain hardening beyond a strain of 0.05. The absence of hardening is consistent with the dislocation dynamics simulation results which were used to construct the dislocation evolution model. It is known that this low strain hardening is not consistent with experimental observation, and efforts are underway to understand why the dislocation density saturates so quickly in the calculations. The apparent strain hardening at the highest strain rates in Figure 7 is a result of temperature increase due to adiabatic heating.

The temperature dependence of the strength is illustrated in Figure 8. Figure 8a is constructed at a strain rate of 10^2 sec^{-1} where thermal activation is the dominant mechanism. The flow strength is reduced as the temperature increases. Figure 8b is constructed at a strain rate of 10^6 sec^{-1} where phonon drag is dominant. Here the trend of strength with temperature is reversed. At higher temperature the crystal lattice vibrations are larger, providing a greater impediment to dislocation motion. This temperature strengthening effect, combined with adiabatic heating, is responsible for the apparent hardening seen at the highest rate in Figure 7b. Because of the change in mechanisms, it is expected that the model will exhibit very little temperature sensitivity at some strain rate intermediate between these two.

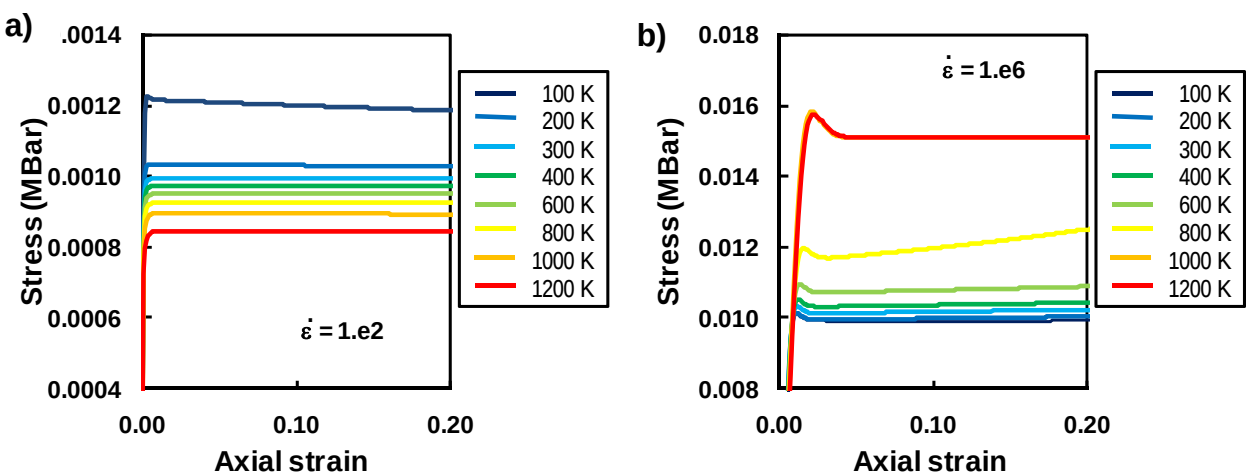

Figure 8. Temperature dependence of strength at strain rates of a) 10^2 sec^{-1} and b) 10^6 sec^{-1} illustrating the different behavior in, respectively, the thermally activated and phonon drag regimes.

The pressure dependence of the model is through combined influence of the shear modulus, activation energy (Eq. 4), Peierl's stress (Eq. 5), evolved dislocation density and Orowan relation (Eq. 1). As the pressure is increased, keeping strain rate constant, the dislocation density increases, Figure 9a. The increase is modest but consistent. The flow strength, on the other hand, shows an unanticipated trend of decreasing as pressure is increased, Figure 9b. Examining the results in closer detail reveals that the dislocation velocity increases slightly with pressure implying that the reduction in velocity balancing the increased dislocation density in Orowan's equations is not entirely responsible for the downward trend in stress. The pressure dependence of the activation energy and Peirels stress also contribute to the strength reduction. While the effect is small, it does highlight the highly interdependent nature of the model.

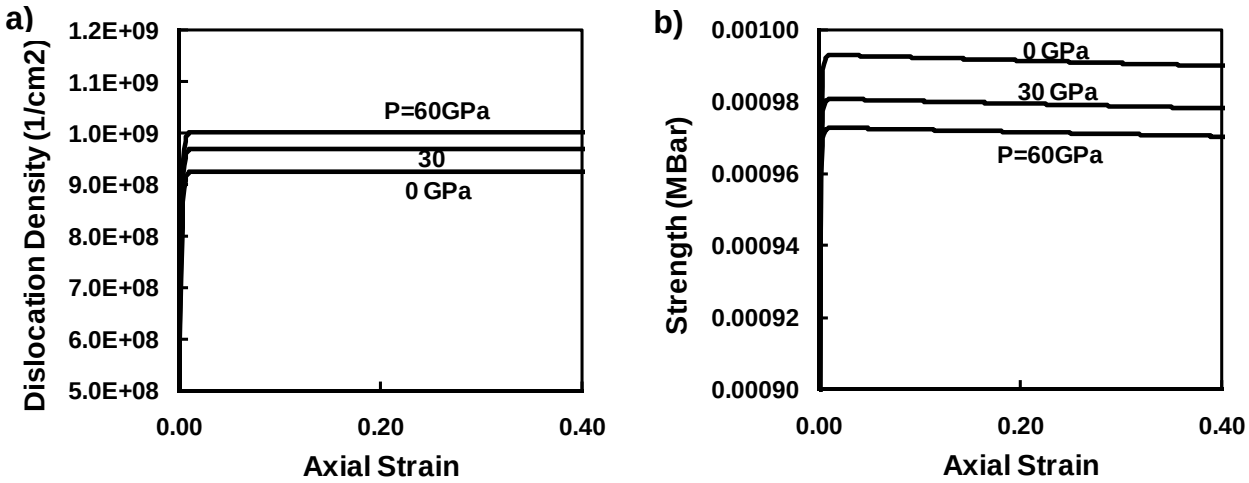

Figure 9 Evolution of a) dislocation density and b) flow strength at pressure and at a strain rate of 100 sec^{-1}

Closing remarks

Constructing continuum level models using an array of multiscale simulations is an evolving process. Several lessons learned from the prior tantalum work[1] have been applied here, and experience from the current vanadium model will be applied to future models. The most significant advancement in the current model has been use of dislocation kinetic relations determined from molecular dynamics simulations. This provided constants for the kinetic relations and data to fit for the transition from thermal activation to phonon drag. An attempt was made to utilize distinct history variables for edge and screw dislocations, but the lack of direct coupling between the two evolving populations lead to instabilities and unphysical behavior.

Discoveries and experiences from the current model suggest modifications to the procedure for future models. The few suggestions provided below are conservative in that they aim to extract more information from existing simulation capabilities rather than developing new capabilities.

- It is evident that kinetic relations determined from the molecular dynamics simulations do not fit with a strict Arrhenius model. The activation energy is likely temperature dependent. This suggests that more latitude can be taken in choosing a functional form for the kinetic relation.
- Direct use of the dislocation kinetic relations in the continuum model neglects the distribution of dislocation velocities and dislocation interactions. The dislocation dynamics code was constructed to include these effects and average the behavior. Running ParaDiS through jump tests in strain rate, pressure and temperature will provide these dependencies directly in terms of macroscopic stress and plastic strain rate. Jump tests are needed to extract the relations at constant dislocation structure.
- The pressure dependence of the strength is contrary to the direction suggested by the limited experimental data available. A path forward is to use a range of pressures when running MD simulations determining dislocation kinetic relations. This will avoid extrapolating pressure dependence of the activation energy over a range of temperatures.

Acknowledgements

We would like to thank Bruce Remington for valuable feedback. Support of the ASC-PEM program is gratefully acknowledged. This work performed under the auspices of the U.S. Department of Energy by Lawrence Livermore National Laboratory under Contract DE-AC52-07NA27344. LLNL-TR-416095

References

[1] Arsenlis, A., "L2 Multiscale Strength Milestone Review," *Presentation to the L2 Milestone committee*, 2007

[2] Arsenlis, A., "ASC L2 Milestone: Multiscale Modeling of Vanadium Strength," *Presentation to the L2 Milestone committee*, 2008, LLNL-PRES-407164

[3] Yang, L.H., Per Söderlind, P and Moriarty, J.A., "Accurate atomistic simulation of (a/2) <111> screw dislocations and other defects in bcc tantalum," *Phil. Mag. A*, **81**, 2001, pp. 1355-1385.

[4] Yang, L.H., Tang, M. and Moriarty, J.A., "Dislocations and Plasticity in bcc Transition Metals at High Pressure," Chapter 92 in Dislocations in Solids, Eds J.P. Hirth and L. Kubin, Elsevier B.V., 2010.

[5] Marian, J., Cai, W. and Bulatov, V. V., "Dynamic transitions from smooth to rough to twinning in dislocation motion," *Nature Materials*, **3**, 2004 pp. 158-163.

[6] Marian, J. and Caro, A., "Moving dislocations in disordered alloys: Connecting continuum and discrete models with atomistic simulations," *Phys. Rev. B*, **74**, 2006, 024113.

[7] Aresnlis, A., Cai, W., Tang, M., Rhee, M., Oppelstrup, T., Hommes, G., Pierce, T.G. and Bulatov, V.V., "Enabline strain hardening simulations with dislocation dynamics," *Modelling Simul. Mater. Sci., Eng.*, **15**, 2007, pp. 553-595.

[8] Bulatov, V.V., Hsiung, L.L., Tang, M., Arsenlis, A., Bartelt, M.C., Cai, W., Florando, J.N., Hiratani, M., Rhee, M., Hommes, G., Pierce, T.G. and Diaz de la Rubia, T., "Dislocation multi-junctions and strain hardening," *Nature*, **440**, 2006, pp. 1174-1178.